Fuel 260 (2020) 116365

Contents lists available at ScienceDirect

Fuel

journal homepage: www.elsevier.com/locate/fuel

Full Length Article

Combustion parameters optimization of a diesel/natural gas dual fuel engine using genetic algorithm

Jie Liu[a,b,*], Biao Ma[a,b], Hongbo Zhao[a,b]

[a] Department of Power Mechanical Engineering, Beijing Jiaotong University, Beijing 100044, PR China
[b] Beijing Key Laboratory of New Energy Vehicle Powertrain Technology, Beijing 100044, PR China

ARTICLE INFO

Keywords:
Optimization
Genetic algorithm
Natural gas
Dual fuel

ABSTRACT

The objective of this study is to optimize the diesel injection parameters, operating parameters and the combustion system of a diesel/natural gas fueled dual fuel engine simultaneously by applying the genetic algorithm. The indicated specific fuel consumption, NO*x* and CH_4 emissions are selected as the optimization objectives. It is shown that almost all the solutions can meet the EURO VI emission limit of the Soot. However, only partial solutions satisfy the EURO V NO*x* emission limit. More open combustion chambers are chosen than the re-entrant combustion chamber on the Pareto front. A wide range distribution of the combustion bowl radius is found on the Pareto front. However, the diesel fuel spray angle, swirl ratio, EGR (Exhaust Gas Recirculation) rate and compression ratio are gradually concentrated near several optimal points. The response surfaces of ISFC, CH_4 and NO*x* emissions for injection timing vs. EGR rate and spray angle vs. swirl ratio for all the calculated Pareto citizens are achieved.

1. Introduction

With the increasingly serious environmental pollution and shortage of petroleum resources, how to improve the thermal efficiency of internal combustion engines while reducing emissions has attracted more and more attention. By using advanced combustion technologies, the NO*x* and Soot emissions can be simultaneously minimized, and the thermal efficiency will be improved without after-treatment systems. However, several challenges still exist in the advanced combustion engines with single fueled, such as difficulty in combustion phase control [1], low combustion stability [2], narrow operation ranges [3], high level of NO*x* emissions [4], and large amounts of PM (particulate matter) emissions for diesel engine [5]. The dual-fuel compression ignition combustion modes, such as Reactivity Controlled Compression Ignition (RCCI) [6] and pilot ignited dual-fuel combustion [7], are considered as a more competitive concept to overcome the above drawbacks of the single fueled advance combustion concepts [8,9].

Shu et al. revealed that the peak cylinder pressure of a natural gas-diesel dual fuel engine increased as the spray angle was increased, but it decreased slightly as the spray angle increases over than 140° [10]. Yousefi et al. suggested that increasing the swirl ratio can obviously improves the combustion process, which consequently enhances fuel efficiency [11]. Yang et al. suggested that a stratified mixture could be achieved with late natural gas injection in cylinder, which can provide a way to increase the combustion efficiency and reduce THC and CO emissions [12]. Shim et al. showed the possibility of reducing HC and CO emissions, while increasing combustion efficiency simultaneous by using optimized intake charge strategies [13]. Ryu showed that advancing the diesel injection timing at low load and delaying the diesel injection timing at high load will improve the performance of dual fuel engine [14]. Liu et al. revealed that the total hydrocarbon emissions were reduced obviously when the quantity of the pilot diesel was increased [15]. Papagiannakis et al. reported that the NO emissions were increased, whereas the CO emissions and fuel consumption rate were reduced with advancing the pilot diesel injection timing [16]. Yousefi et al. showed that advancing diesel injection timing could make the thermal efficiency and the NO*x* emissions worse [17]. Yang and Zeng indicated that natural gas injection timing and injection strategy had a significant influence on the engine performance and THC, CO and NO*x* emissions in dual-fuel engines [18]. Wang et al. indicated that significant advancing fuel injection timing would generate a two-stage auto-ignition mode, which will achieve higher thermal efficiency and lower NO*x* and THC emissions simultaneously [19]. Jung et al. reported that the brake power and the NO*x* (nitrogen oxide) emissions were both decreased with the increase of premixed natural gas because of a lower temperature in the cylinder [20]. The low combustion efficiency of NG for the NG-diesel dual fuel engine was mainly due to the emissions of unburned CH_4, and the contribution of CO emissions to the deficiency

* Corresponding author at: Department of Power Mechanical Engineering, Beijing Jiaotong University, Beijing 100044, PR China.
E-mail address: ljie@bjtu.edu.cn (J. Liu).

https://doi.org/10.1016/j.fuel.2019.116365
Received 17 August 2019; Received in revised form 3 October 2019; Accepted 5 October 2019
Available online 13 October 2019
0016-2361/

Nomenclature and list of abbreviations

RCCI	Reactivity Controlled Compression Ignition
BTDC	Before Top Dead Center
ATDC	After Top Dead Center
SOC	Start of Combustion
THC	Total Hydrocarbon
ISFC	Indicated Specific Fuel Consumption
IVC	Intake Valve Closure
CR	Compression Ratio
CNG	Compressed Natural Gas
TD	Throat diameter
BD	Bottom diameter,
IT	Injection timing
SA	Spray angle
CR	Compression ratio
SR	Swirl ratio

of NG combustion was relatively small [21].

Numerous optimization methods were used for the optimization of the performance and emissions of the dual fuel engines. The combination of artificial neural network (ANN) and non-dominated sorting genetic algorithm II (NSGA-II) was employed for the reduction of NO*x* emissions in a direct injection dual-fuel engine [22]. The multi-objective genetic algorithm and the non-linear programming by quadratic Lagrangian (NLPQL) method have been employed for the combustion bowl optimization of a dual-fuel engine [23]. The operating parameters of a syngas/diesel RCCI engine were optimized by integrating the KIVA-3V code with the NSGA-II [24]. The combustion chamber geometry was optimized by using the multi-objective code NSGA-II with Kriging-based meta-model for a diesel/natural gas dual fuel engine [25]. The NSGA-II code was employed for the optimizations of a diesel/natural gas dual fuel engine [26]. A two-stage evolutionary computational approach integrating the NSGA-II and technique for order preference by similarity to ideal solution was developed for the optimization of a dual fuel engine [27].

To date, the combination effect of the injection parameters, operating parameters and combustion chamber profiles on the performance and emissions characteristics of the dual fuel engines has been rarely studied. The main objective of this study is to find the optimal dual fuel engine combustion system with coupled parameters using the artificial intelligence method: genetic algorithm. The newly developed genetic algorithm NSGA-III was used along with the KIVA-3V code for the dual fuel engine optimizations. A total number of 8 parameters were optimized simultaneously, which includes fuel injection parameters, operating parameters and combustion chamber profile parameters.

2. Experimental setup

In this section, the specification of the tested engine was introduced. In addition, the engine exhaust gas measurement equipment and the test method were given. Furthermore, the properties of the tested fuels were introduced.

2.1. Engine specifications

The six-cylinder WEICHAI WP10 diesel engine was modified for the dual fuel combustion mode test. The dual fuel engine specifications are summarized in Table 1. Natural gas was introduced through an additional gas supply system and mixed with air through a mixer, which was installed in the main intake pipe of the engine. An additional dual-fuel control unit was employed to control the injection strategies (injection timing, injection duration, etc) of the diesel fuel and natural gas.

2.2. Instrumentation introduction

The power and torque of the engine were measured by using the Horiba-Schenck HT350 AC dynamometer. A piezoresistive pressure sensor is installed in the first cylinder head for the cylinder pressure acquisition together with the Kistler 5018 charge amplifier. The Horiba MEXA7100DEGR analyzer was employed for the engine out emissions measurement. The total hydrocarbon (THC) and CH_4 emissions were both detected by the Horiba MEXA7100-DEGR analyzer with flame ionization detector (FID). In order to measure CH_4 emission, the selective combustion technology was used in FID, which can separate methane and non-methane hydrocarbons. The test THC emissions including both unburned methane and diesel produced UHC. The mass flow rates of the diesel and compressed natural gas were measured by an ONOSOKKO FZ2100 and a BROOKS mass flow meter, respectively.

2.3. Properties of the test fuels

The diesel fuel and the compressed natural gas were both obtained from the local gas stations. The detailed specifications of these two fuels can be found in Table 2.

3. CFD calculation methodology

In this section, the selected models in the KIVA-3V code used for the simulations were firstly introduced. After that, the coupled combustion model developed by coupling the turbulent flame speed closure model with the PaSR (Partially Stirred Reactor) combustion model was briefly described. Furthermore, the automatic mesh generation method was given. In addition, the algorithm of the newly developed NSGA-III code and the coupling method of the NSGA-III with the KIVA-3V code were presented.

3.1. Models used in the KIVA code

The primary and secondary spray droplet breakups were simulated by the KH-RT (Kelvin- Helmholtz instability theory and Rayleigh-Taylor instability theory) breakup model [28]. The collision and coalescence process between droplets was solved by using the O'Rourke collision model [29]. The turbulence was described by the RNG k-ε method. A blended fuel with 70% n-heptane and 30% toluene (both in vol. basis) was used to represent diesel fuel. In addition, a mixture with four-component of methane, ethane, propane and butane was used to represent the natural gas. A well validated diesel/natural gas dual fuel reaction mechanism with 81 species and 421 elementary reactions was employed for the fuel oxidation calculation [30]. The soot formation and oxidation process were simulated by the Hiroyasu model and the Nagle/Strickland-Constable model, respectively [31]. Moreover, the soot surface growth was accounted by the HACA (Hydrogen-Abstraction/Carbon-Addition) mechanism. The NO*x* formation was simulated

Table 1
Specifications of the dual fuel engine.

Bore × Stroke	126 × 130 mm
Cylinder number	6
Displacement	9.726 L
Rated power/speed	247 kW/2200 rpm
Compression ratio	17.0
Number of Injector nozzle holes	7
Spray angle	146°
Exhaust valve opening timing	131 °CA ATDC
Inlet valve closing timing	146 °CA BTDC

Table 2
Specifications of the test fuels.

CNG		0# diesel	
Methane	96.51% v/v	Cetane number	52.6
Ethane	1.2% v/v	Density	833.7 kg/m^3
Propane	0.18% v/v	Lower heat value	42.74 MJ/kg
Butane	0.04% v/v	Stoichiometric air–fuel ratio	14.5 kg/kg
Lower heat value	50.9 MJ/kg		
Stoichiometric air–fuel ratio	16.88 kg/kg		

by the extended Zel'dovich NO*x* mechanism [32], as shown in Table 3.

3.2. Coupled combustion model

Generally, there are two combustion stages in the dual fuel combustion engine. The first stage is the ignition and combustion of the injected diesel fuel, which is similar with the combustion process in traditional diesel engine. In this case, the first combustion stage can be simulated by the PaSR combustion model, which was widely used in diesel engine combustion simulation [32]. However, the second stage is the flame propagation process in the premixed natural gas/air mixture, which cannot be effectively predicted by using the PaSR model alone. Therefore, the TFSC (turbulent flame speed closure) combustion model was introduced to simulate the flame propagate process in the premixed mixture, and it was coupled with the PASR combustion model. The species conservation equation of the coupled combustion model can be written as follows:

$$\frac{\partial c_m}{\partial t} + \nabla\cdot(\mathrm{c_m}\mathbf{u}) = \nabla\cdot\left[\rho \mathrm{D}\nabla\left(\frac{\mathrm{c_m}}{\rho}\right)\right] + \dot{\rho}_{\mathrm{m}}^{\mathrm{c1}} + \dot{\rho}_{\mathrm{m}}^{\mathrm{c2}} \tag{1}$$

where the chemical reaction source terms of the TFSC model and the PaSR model are given as $\dot{\rho}_m^{c1}$ and $\dot{\rho}_m^{c2}$, respectively. c_m represented the mass fraction of the species presented in the mixture.

The conservation equation for the turbulent flame speed closure model is:

$$\frac{\partial}{\partial t}(\bar{\rho}\tilde{c}) + \nabla\cdot(\bar{\rho}\tilde{\mathrm{c}}\mathbf{u}) = \nabla\cdot[\bar{\rho}\mathrm{D}\nabla\tilde{\mathrm{c}}] + \rho_\mathrm{u}\mathrm{S_t}\,|\nabla\tilde{\mathrm{c}}| + \bar{\rho}(1-\tilde{\mathrm{c}})\Big/\tau_\mathrm{f} \tag{2}$$

The density with the subscript u stands for the unburned mixture density. The turbulent flame propagation speed is represented by S_t, which is depending on the local laminar flame velocity and the turbulence characteristics, e.g., $u'\sim k^{1/2}$ [33]. The combustion process variable c is used to describe the extent of combustion process, where 0 means the unburned gas and 1 represents the equilibrium products.

The unified chemical time for the new developed combustion model is written as follows:

$$\tau_c = \frac{\tau_{c1}\tau_{c2}}{\tau_{c1}+\tau_{c2}} \tag{3}$$

The detail description of the combustion model was presented in our previous research [34].

3.3. Parameterized piston model

In order to investigate the effect of combustion bowl geometries on the performance and emissions characteristics of the dual fuel engine, the automatic mesh generation technology need to be adopted. The basic ideas are as follows: the piston bowl profile was divided into a sequence of arcs, straight lines and so on. The tangent restrictions were applied for these segments at the connection points, which were noted as the control points. The adjustment of the combustion chamber geometry was accomplished by changing the location of these control points, which were derived from the input geometry variables (optimization parameter). Fig. 1 displays the combustion chamber geometry parameters and the control points, which are used for the auto mesh generation. The height of the central pip, the throat and the bottom radius are represented by H_1, R_1 and R_2, respectively. H_2 is the piston bowl depth, which is varied to match the target compression ratio.

3.4. Optimization procedure

As most of the engineering problems have to meet several objectives, it is impossible to obtain a unique solution that satisfies all the objectives simultaneously. Usually, the evolutionary multi-objective optimization (EMO) algorithms, which have been certificated their usefulness in solving multi-objective optimization problems, are employed to solve the engineering optimization problems. The Non-dominated Sorting Genetic Algorithm (NSGA) was one of these evolutionary algorithms. Over the years, the elitism was introduced and an explicit diversity preserving mechanism was added to make it more suitable in practical problem, which was usually referred to as NSGA-II [35].

In recent years, an evolutionary optimization algorithm NSGA-III, which was based on the NSGA-II procedure, was developed for solving the multi-objectives problems [36]. Basically, the frameworks of the NSGA-II and NSGA-III were similar. But unlike in NSGA-II, significant changes were made in the selection mechanism in NSGA-III. In NSGA-II, the maximum diversity of the Pareto-optimal front was achieved through a niche-preservation operator which computed the 'crowding distance' between two neighboring results, where the crowding distance of the solution is the average side-length of the cuboid in its front, as shown in Fig. 2(a) with a dashed box. The result with the larger 'crowding distance' will be chosen as the preferred solution, as shown in Fig. 2(a) for two-objective problems. However, in NSGA-III, a set of widely distributed points was introduced first to the entire solutions space. The algorithm was to find the preferable solutions with the smaller distance to the reference points (lines), as shown in Fig. 2(b). In this case, the chosen solutions were probably to be widely distributed on the Pareto front.

The overall coupling method of the NSGA-III with KIVA-3V and the auto mesh generation codes is given in Fig. 3. Firstly, the 8 optimization parameters were randomly generated by the NSGA-III code within the variables ranges. Thereafter, the parameters of fuel injection timing and spray angle, swirl ratio and the EGR rate were sent to the KIVA code. Meanwhile, three bowl geometry parameters and the compression ratio were collected by the auto mesh generation code for the combustion bowl mesh generation. Secondly, the dual fuel engine combustion process was calculated by the KIVA-3V code using the newly generated

Table 3
Elementary steps in the thermal mechanism of NO and N_2O. Units are cm^3–mol–s–cal–K, and $k = AT^n\exp(-E_a/RT)$.

No.	Reaction	*A*	*n*	E_a
1	$N + NO = N_2 + O$	3.50E + 13	0	330
2	$N + O_2 = NO + O$	2.65E + 12	0	6400
3	$N + OH = NO + H$	7.33E + 13	0	1120
4	$N + CO_2 = NO + CO$	1.90E + 11	0	3400
5	$N_2O + O = N_2 + O_2$	1.40E + 12	0	10,810
6	$N_2O + O = NO + NO$	2.90E + 13	0	23,150
7	$N_2O + H = N_2 + OH$	4.40E + 14	0	18,880
8	$N_2O + OH = N_2 + HO_2$	2.00E + 12	0	21,060
9	$N_2O + M = N_2 + O + M$	1.30E + 11	0	59,820
10	$NO + HO_2 = NO_2 + OH$	2.11E + 12	0	−480
11	$NO_2 + O = NO + O_2$	3.90E + 12	0	−240
12	$NO_2 + H = NO + OH$	1.32E + 14	0	360
13	$NO + O + M = NO_2 + M$	1.06E + 20	−1.41	0
14	$NO_2 + CH_3 = CH_3O + NO$	1.50E + 13	0	0
15	$NO + CH_3O_2 = NO_2 + CH_3O$	2.53E + 12	0	−358

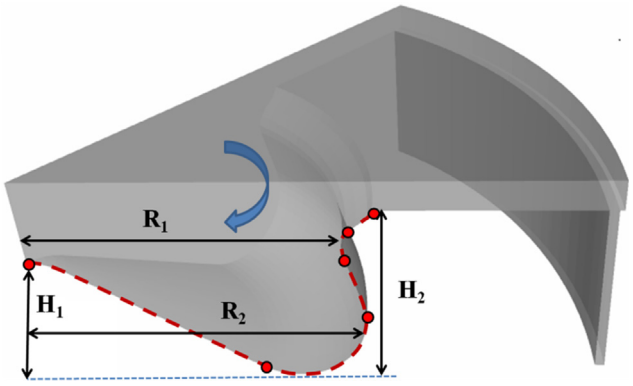

Fig. 1. Definition of control points and parameters of the combustion chamber.

combustion chamber and the initial conditions. Then, the calculated engine emissions and economic data were read by the NSGA-III code. Thirdly, all calculation results of the present generation were mixed with the previous set of the optimal solutions. The NSGA-III code will evaluate these solutions and find the favorable solutions to forming the new Pareto front for the present generation. After that, the populations for the next generation will be created through the selection, crossover and mutation method. This loop will continue to reach the maximum generations iteration. The optimal solution can be found on the last Pareto front.

Three objectives were chosen for the optimization, which were the ISFC, NO*x* emission and CH_4 emission. A total number of 8 parameters were chosen as the variables during the optimization process, including injection parameters, operating parameters and combustion bowl profile parameters. The ranges chosen for these 8 variables during the optimization process are listed in Table 4. In this study the cooled EGR is used to study the effect of EGR ratio on the combustion and emission characteristics of the dual fuel engine. The temperature of the EGR is set to be the same as that of the intake air. The exhaust gas contains only CO_2 and H_2O. Based on the EGR rate definition of Hamosfakidis and Reitz [37], when the EGR load is specified, the intake mole fractions of the CO_2 and H_2O in the intake air can be calculated using linear interpolation formulas:

$$[CO_2]_{Intake} = EGR(\%)/100.*[CO_2]_{Exhaust} + (1. - EGR(\%)/100.)*[CO_2]_{Ambient} \quad (4)$$

$$[H_2O]_{Intake} = EGR(\%)/100.*[H_2O]_{Exhaust} + (1. - EGR(\%)/100.)*[H_2O]_{Ambient} \quad (5)$$

where $[CO_2]_{Intake}$ and $[H_2O]_{Intake}$ are the intake mole fractions of CO_2 and H_2O. $[CO_2]_{Exhaust}$ and $[H_2O]_{Exhaust}$ are the exhaust mole fractions of CO_2 and H_2O, which are selected from the equilibrium condition. $[CO_2]_{Ambient}$ and $[H_2O]_{Ambient}$ are the mole fractions of CO_2 and H_2O in the ambient air. $EGR(\%)$ is the EGR rate.

Five constraints were employed to exclude the irrational cases in the optimal solution selection. The peak combustion pressure, maximum rate of pressure rise and acceptable ISFC were limited to less than 20 MPa, 2 MPa/°CA and 250 g/kW·h, respectively. Moreover, the misfire and abnormal termination cases were also excluded during the optimal solution selections [26].

4. Results and discussions

In this section the selected computational fluid dynamics and combustion models will be validated with the experimental data. After that, all the calculation result and the optimal solutions on the Pareto front will be given. In addition, the regression analysis of the parameters will be conducted. Finally, the effect of the combustion bowl geometry on the spatial distributions of the temperature, pollution fractions and the flow field will be analyzed.

4.1. Validation of the calculation method

To begin with, three meshes (cell size 0.10, 0.15 and 0.2 cm) were used to check the sensitivity of the cell size on the calculation result of the diesel/natural gas dual fuel engine. It was found that only very small difference was appeared when the cell length in the radial direction was less than 1.5 mm (the maximum length of the cell in the axial direction was 1 mm for all the three meshes), as shown in the previous research [26]. In order to save the calculation time and keep accuracy, the 0.15 cm mesh was employed to simulate combustion process of the dual fuel engine. The cylinder pressures and heat release rates predicated by this mesh agreed well with the experimental data, as shown in Fig. 4. In addition, the simulated NO*x* emission, CH_4 emission and CO emission were shown good agreement with the experimental data, as shown in Fig. 5. The CH_4 emission is mostly due to the retention of unburned fuel in squish and crevices regions in the cylinder. Natural gas mixed with air is compressed into the crevices during the compression stroke and is released during the expansion process. Most of it is exhausted in the unburned form. The details of the crevices model was not include in our simulations, so there will be some deviations for the calculation results. Furthermore, the dual fuel engine is modified from the diesel engine, where the large valve overlap angle is employed to increase the scavenging efficiency and some of the premixed natural gas may be discharged from the cylinder. The CO is a major product in the final stages of the hydrocarbon oxidation, requiring the inclusion of the various oxidation pathways from the pure fuel to the final oxidized products. The natural gas combustion mechanism implemented in KIVA is validated based on experimental shock tube data. While correct ignition delay guarantees correct radicals formation to initiate the combustion, it does not guarantee that all pathways leading to CO formation are considered throughout the

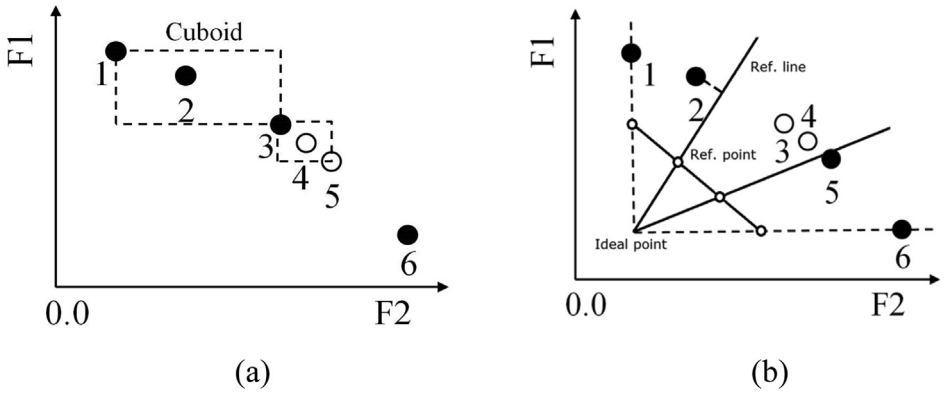

Fig. 2. Comparison of the selection principles of the NSGA-II and NSGA-III codes.

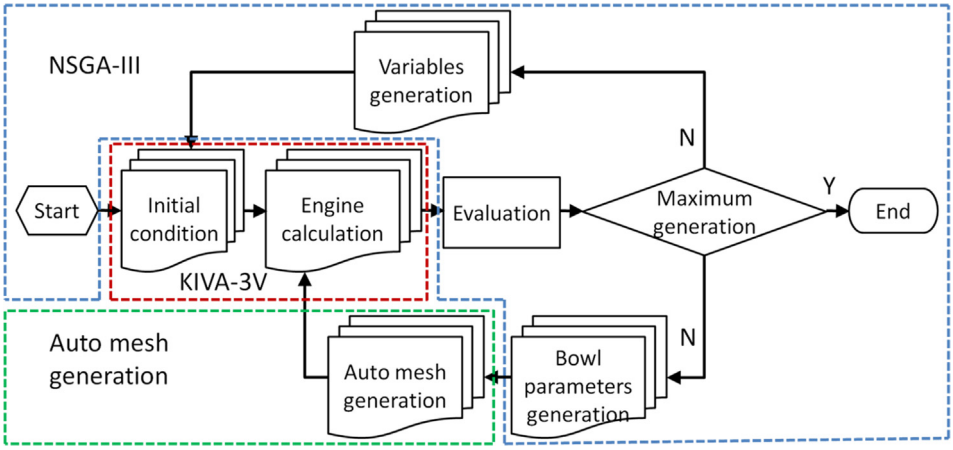

Fig. 3. The coupled computational flow chart of the optimization process.

Table 4
The variables and ranges selected for the optimization.

Variables	Minimum	Maximum	Original
Injection timing/°CA BTDC	−40	0.0	−7.5
Spray angle/°	90	160	146
Height of central pip/cm	0.5	1.525	1.525
Throat radius/cm	3.5	4.5	3.765
Bottom radius/cm	3.3	4.8	3.69
Swirl ratio	0.5	2.0	1.4
Compression ratio	15.0	19.0	17.0
EGR rate	0.0	30%	0.0

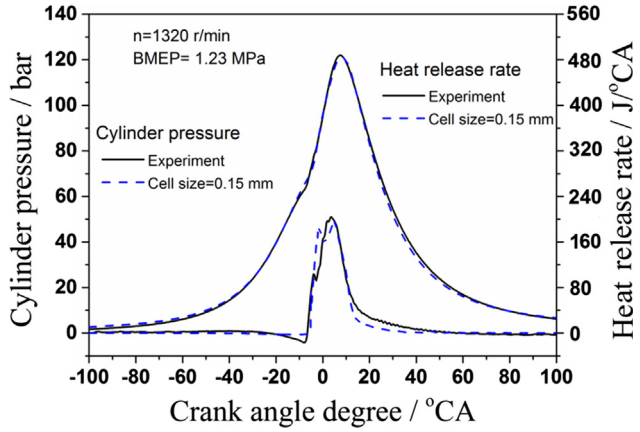

Fig. 4. Comparisons of the calculation and experimental pressures and the heat release rates.

combustion mechanism. Investigating the details of the combustion mechanism is beyond the scope of this work; however, the current results indicate that further improvements to the mechanism are needed for better prediction of CO.

4.2. Optimization results of the dual fuel engine

All the calculated citizens and the citizens on the Pareto front are presented in Fig. 6. It is shown that the solutions are widely distributed in the three-dimensional objective space. As indicated in the Pareto citizens, the NSGA-III algorithm using the evolutionary optimization methods is capable to find the leading front closest to the ideal point and the diversity is ensured in the obtained optimal solutions. Further observation revealed that the fuel consumption rate and emissions were reduced significantly compared with the optimal solutions and that of the original engine.

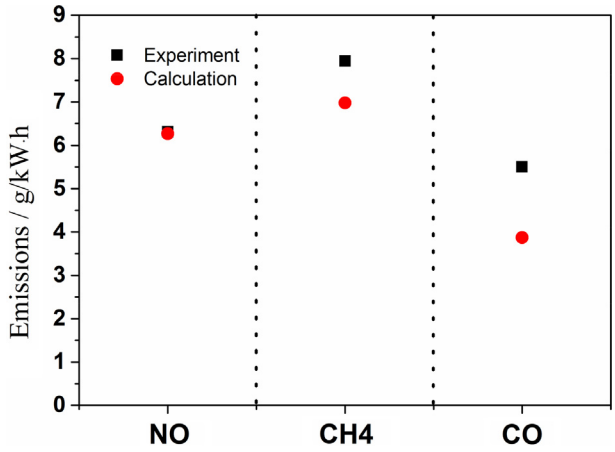

Fig. 5. Comparisons of calculation and experimental NO*x*, CH_4 and CO emissions.

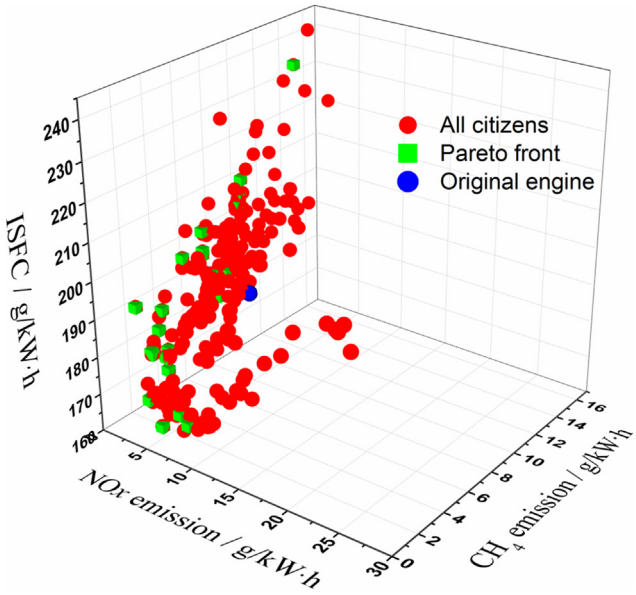

Fig. 6. Comparison of all calculated citizens and the cases on the Pareto front.

The ISFC was calculated with the equivalent diesel fuel consumption rate, which was based on the lower heating values of the diesel and natural gas. The formula is as follows:

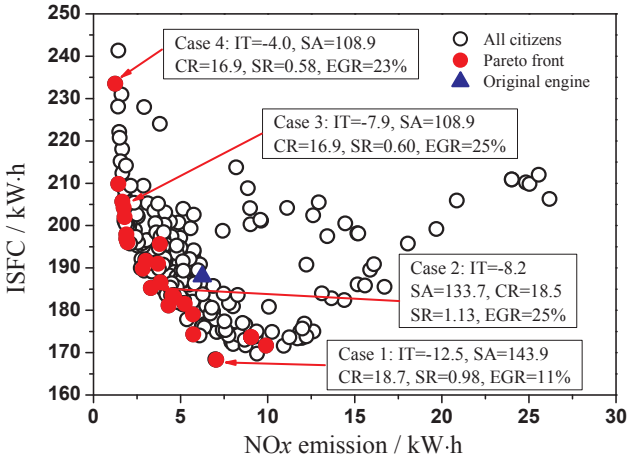

Fig. 7. The relations between ISFC and NO*x* emission of the calculated cases.

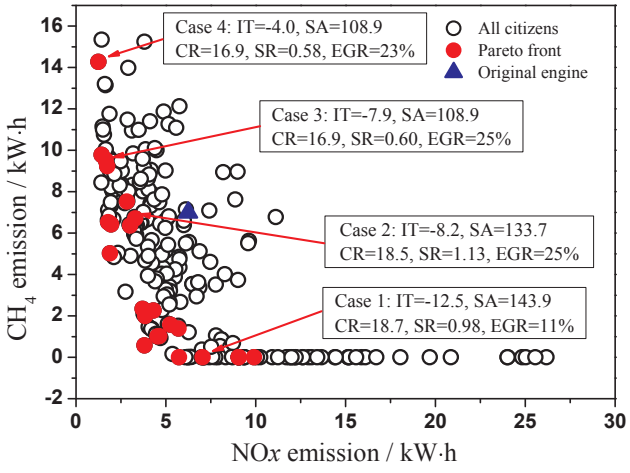

Fig. 8. The relations between NO*x* and CH_4 emission of the calculated cases.

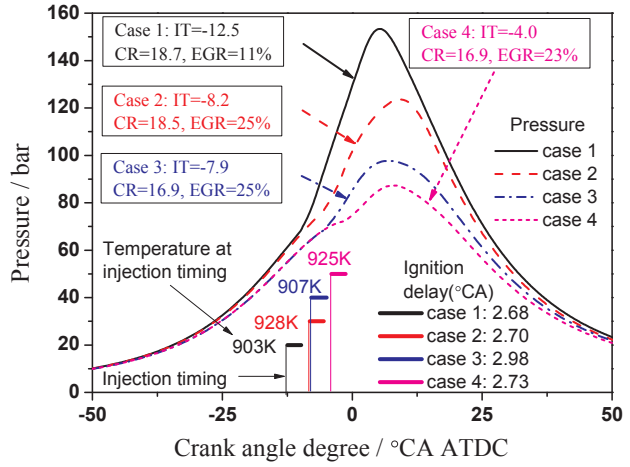

Fig. 9. Cylinder pressures of the four selected cases.

$$\mathrm{ISFC} = \frac{H_{\mathrm{LD}}B_{\mathrm{D}} + H_{\mathrm{LG}}B_{\mathrm{G}}}{H_{\mathrm{LD}}P_{\mathrm{e}}} \quad (4)$$

where H_{LD} and H_{LG} are the lower heating value of diesel fuel and natural gas, respectively. B_{D} and B_{G} are the consumption rate of diesel fuel and natural gas. P_{e} is the brake power of the engine.

The ISFC versus NO*x* emissions of the obtained solutions are shown in Fig. 7. The trade-off relations between them are clear from the plot.

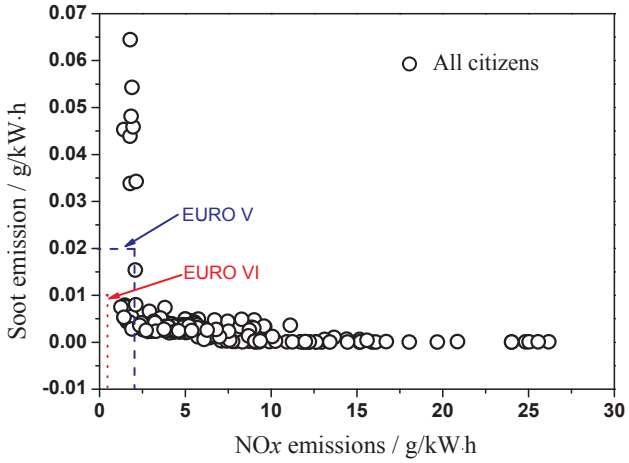

Fig. 10. The limited pollution emission space of the dual fuel engine.

The reduction of ISFC will cause an increased NO*x* emission and vice versa. The solutions on Pareto front have advantages in both ISFC and NO*x* emissions compared with the other solutions. Four cases on the Pareto front are chosen to demonstrate the effect of the main parameters on the ISFC and NO*x* emissions, as shown in Fig. 7. The minimum ISFC case in the Pareto front is case 1 with an ISFC of 168.3 g/kW•h, nevertheless, the NO*x* emission is around 7.0 g/kW•h at the same time. The fuel injection timing (IT) of case 1 is −12.5 °CA ATDC, the spray angle (SA) is 143.9°, the compression ratio (CR) is 18.7, the swirl ratio (SR) is 0.98 and the EGR rate (EGR) is 11%, as shown in Fig. 7. The NO*x* emission can be further reduced when the parameters are changed to IT = −8.2 °CA ATDC, SA = 66.8°, CR = 18.5, SR = 1.13, EGR = 25% for case 2, and IT = −7.9 °CA ATDC, SA = 54.5°, CR = 16.9, SR = 0.6, EGR = 25% for case 3,where the fuel injection timings are retarded, the spray angles are narrower, the compression ratios are reduced and the EGR rates are increased compared with case 1. The lowest NO*x* emission case is case 4, which has the smallest fuel injection timing, spray angle and compression ratio and almost the largest EGR rate.

Similar to the phenomenon observed between the ISFC versus NO*x* emissions, the reduction of CH_4 emission also causes an increased NO*x* emission, as given in Fig. 8. The minimum CH_4 emissions are close to zero, which indicates the natural gas can be oxidized completely through the flame propagation. Although some cases have very low NO*x* emissions on the Pareto front, plenty of natural gas was not oxidized completely during the combustion process. For example, the CH_4 emissions are over than 6.0 g/kW•h when the NO*x* emission is less than 2.0 g/kW•h as shown on the Pareto front. In addition, the fuel economy will be deteriorated with the increase of CH_4 emissions as the combustion efficiency is reduced. Furthermore, methane is the second most important greenhouse gas after carbon dioxide. Therefore, the CH_4 emissions should be as small as possible. In this case, the fuel injection advance angle should be larger, the spray angle should be broader, the compression ratio should be higher and the EGR rate should be smaller.

The pressure curves and the ignition delay times of case 1 to case 4 are given in Fig. 9. The ignition timing is related to the cylinder temperature, EGR rate, and kinetics [38,39]. The case 1 has the highest compression ratio, lowest EGR rate and earliest diesel injection timing, therefore, the premixed natural gas is ignited at very earlier time, which will result in highest cylinder temperature and promote the combustion process. When the initial condition transits from case 1 to case 4, the compression ratio is decreasing, the EGR rate is increasing and the diesel fuel injection timing is retreating, therefore the ignition timing is significantly delayed. Most of the combustion process is happened after the top dead center, which result in lower cylinder temperature and thermal efficiency. The cylinder temperatures at the injection timing for

Table.5
Optimized parameters in the Pareto front.

	R2-R1 cm	Injection timing °CA	Spyay angle °	Compression ratio —	Swirl ratio —	EGR ratio —	NO*x* g·(kW·h)$^{-1}$	CH_4 g·(kW·h)$^{-1}$	ISFC g·(kW·h)$^{-1}$
1	0.19	−12.54	143.89	18.70	0.98	0.11	7.04	0.00	168.33
2	0.55	−8.19	133.65	18.47	1.13	0.25	3.30	6.70	185.27
3	−0.48	−7.93	108.93	16.91	0.60	0.25	1.66	9.52	205.61
4	−0.47	−4.05	108.93	16.91	0.58	0.23	1.25	14.28	233.50
5	−0.46	−7.93	105.31	16.87	0.60	0.26	1.43	9.78	209.82
6	−0.48	−7.93	108.93	16.91	0.60	0.25	1.74	9.23	204.23
7	0.32	−7.99	119.64	16.18	0.58	0.26	1.79	6.52	201.97
8	0.79	−14.69	107.75	16.81	0.59	0.26	1.89	5.02	197.89
9	0.32	−7.99	119.64	16.87	0.58	0.26	1.89	6.47	196.86
10	0.31	−7.99	119.64	16.91	0.58	0.26	1.95	6.42	196.03
11	0.50	−18.18	108.08	18.95	1.10	0.26	3.82	0.57	195.65
12	−0.47	−12.66	105.64	16.79	0.60	0.25	3.02	6.36	191.64
13	0.76	−19.81	107.72	16.79	0.59	0.25	3.71	2.34	190.98
14	0.55	−4.30	135.90	18.47	1.10	0.23	2.84	7.52	189.82
15	0.60	−18.10	107.73	16.79	0.59	0.25	3.85	1.99	186.59
16	0.85	−20.59	107.75	16.77	0.59	0.26	4.54	1.01	183.46
17	0.64	−20.59	107.73	16.79	0.59	0.25	4.64	1.01	183.02
18	0.87	−20.10	119.40	16.16	0.58	0.26	5.25	1.58	181.52
19	0.65	−12.57	121.78	18.60	1.11	0.25	4.32	2.26	181.11
20	−0.43	−18.66	140.57	17.07	1.14	0.25	5.71	1.39	178.99
21	0.65	−18.07	118.82	18.60	1.12	0.27	5.74	0.00	174.30
22	0.65	−18.07	118.82	18.63	1.12	0.10	9.06	0.00	173.68
23	0.46	−17.02	139.04	18.96	0.92	0.12	9.91	0.00	171.65

case 1–4 are 903 K, 928 K, 907 K and 925 K, respectively. The temperature difference at the injection timing is due to the combined effect of the injection timing, compression ratio and EGR rate. The ignition delay times of case 1, case 2 and case4 are nearly the same, which are all around 2.7 °CA. Case 3 has slight larger ignition delay time compared with the other three cases, which is around 3.0 °CA as it using the lowest compression ratio and highest EGR rate.

In order to find the limited pollution space of the diesel/natural gas dual fuel engine, the Soot versus NO*x* emissions of all obtained solutions are shown in Fig. 10. For Soot emissions, almost all the solutions can meet the EURO VI emission limit (0.01 g/kW•h). However, for NO*x* emissions, only partial solutions can satisfy the EURO V emission limit (2.0 g/kW•h). As the particulate number emission was not included in the Soot model, the particulate number result was not shown in this figure. In this case, the high efficiency SCR (Selective Catalytic Reduction) system should be employed for the development of the EURO VI Powertrain system with the dual fuel engine.

In order to give an explicit optimization result, the values of all the optimized parameters on the Pareto front are given in Table 5.

4.3. Regression analysis of the parameters

In order to estimate the relationship between engine output characteristics with different parameters, the regression analysis was conducted. Fig. 11 shows the response surfaces of ISFC, CH_4 and NO*x* emissions for injection timing vs. EGR rate (a, c, e), and spray angle vs. swirl ratio (b, d, f) for all the calculated citizens. The spray angle is the spray cone angle of the diesel injector. The swirl ratio is defined as the ratio of air r.p.m. to crank shaft r.p.m. The injection timing is the diesel fuel injection crank angle.

The response surface of ISFC for injection timing vs. EGR rate shows an inverted-bell shape, as shown in Fig. 11(a). The minimum fuel consumption rate appears at the center of the response surface. The fuel consumption rate decreases with the increase of the spray angle. The increase of the swirl ratio will increase the ISFC slightly. As a result, the fuel consumption rate can reach a minimum point when the spray angle is the largest and the swirl ratio is the smallest, as shown in Fig. 11(b).

The fuel injection timing is the most significant parameter affecting the CH_4 emissions. With advancing of the injection timing, the CH_4 emission decreases obviously. The CH_4 emission decreases slightly with small amount of EGR additions. However, CH_4 emission will be increased when large amounts of EGR were introduced, as shown in Fig. 11(c). The response surface of CH_4 emissions for spray angle vs. swirl ratio appears as a saddle-like pattern. The CH_4 emissions are very high with very large or small swirl ratios. However, when the spray angle and the swirl ratio reach the maximum design value at the same time, CH_4 emission reaches the minimum point, as shown in Fig. 11(d). In contrast to the methane emissions, the retarded injection timing is the most influential parameter in achieving the reduction of NO*x* emissions. The introduction of EGR rate has a moderate effect on the NO*x* emissions compared with the fuel injection timing, as shown in Fig. 11(e). The response surface of NO*x* emissions for spray angle vs. swirl ratio also shows the saddle shaped pattern too. Under very high or low swirl ratio condition, the NO*x* emission is the lowest. However, NO*x* emissions will grow to a very high value when the spray angle and the swirl ratio reach the maximum design value simultaneously, as shown in Fig. 11(f).

4.4. Evolution of the parameters on Pareto front

The evolutionary trend of the throat radius, maximum bottom radius, pilot fuel injection timing, spray angle, swirl ratio, EGR rate and compression ratio on the Pareto front at each generation are shown in Fig. 12. The differences between the radius at the throat and bottom position of the chamber at each generation are shown in Fig. 12(a). The cases with negative radius difference are the re-entrant combustion chamber, and positive cases are called as the open combustion chamber. The open and re-entrant combustion chambers are both appearing on the Pareto front, which means they all have advantages with respect to the three objectives. It should be noticed that large number of open combustion chambers are chosen than the re-entrant combustion chamber. Excessive advancing fuel injection timing is not conducive to improving engine performance, as the fuel injection timing are all constrained to less than 20 °CA BTDC. As the evolution progresses, the diesel fuel spray angles gradually converge to three values, which are around 108°, 120° and 140°. The swirl ratios on the Pareto front gradually degenerate to two points, which are around 0.6 and 1.0. The EGR rates are divided into two grades, which are around 10% and 25%. Three compression ratios are favorable on the Pareto front, which are around 16.1, 16.8 and 18.7.

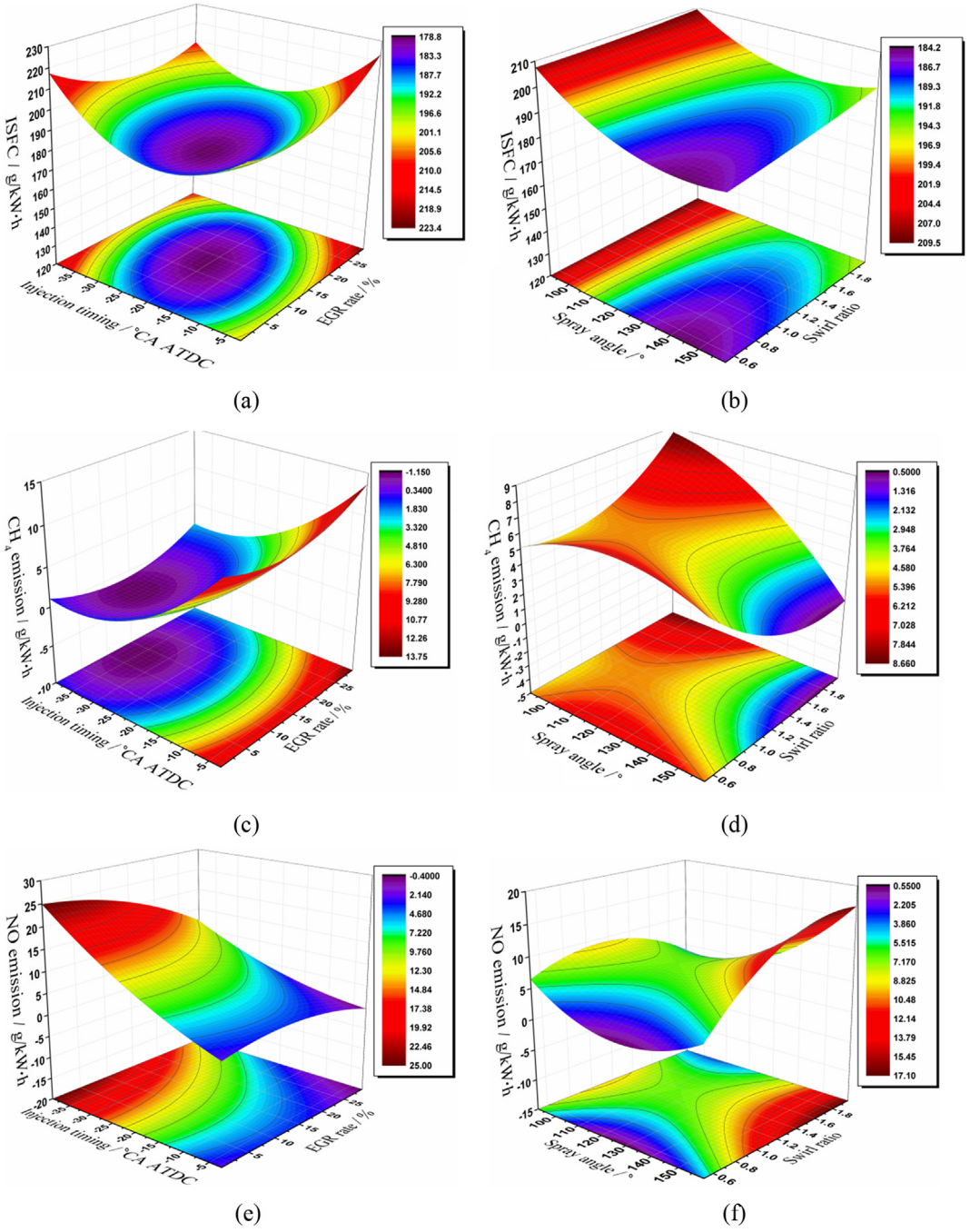

Fig. 11. Response surfaces of ISFC, CH_4 emission, NO*x* emission and the main parameters.

4.5. The temperature and pollutions distributions

Two cases on the Pareto front with different combustion geometries are selected to study the effect of the combustion bowl geometry on the in-cylinder temperature and pollution spatial distributions. The comparison of the parameters chosen for these two selected cases is given in Table 6. In case 1, the open chamber case, the injection timing is about 4.6 °CA earlier than that of the re-entrant chamber (case 3). In addition, the spray angle, compression ratio and the swirl ratio of case 1 are also larger than that of case 3. Meanwhile, the EGR rate in case 1 is less than that of the case 3. These chosen parameters make case 1 lies in the low ISFC area, which is around the center of the response surface as shown in Fig. 11. The high EGR rate, low swirl ratio, low compression ratio and small injection advance angle make case 3 lies in the extreme low NO*x* emissions area. However, the CH_4 emissions and ISFC are very high in this area. As the crevice model was not included in the model, the methane emissions could be very low, as in case 1.

In order to further explore the emission formation process, the temporal and spatial distribution of temperature and pollutants of these two cases are given in Fig. 13. As the fuel injection timing is earlier in case 1, the high temperature area almost occupies the entire combustion chamber at the top dead center, whereas the high temperature region is only distributed at the bottom of the combustion chamber in case 3. When the piston further goes down, the flame can easily propagate into the squish region and ignite the fuel-air mixture there in case 1 as the flow resistance is low in the wide opening throat region, while the small throat diameter in case 3 will change the flow direction and keep the high temperature region in the combustion chamber. The

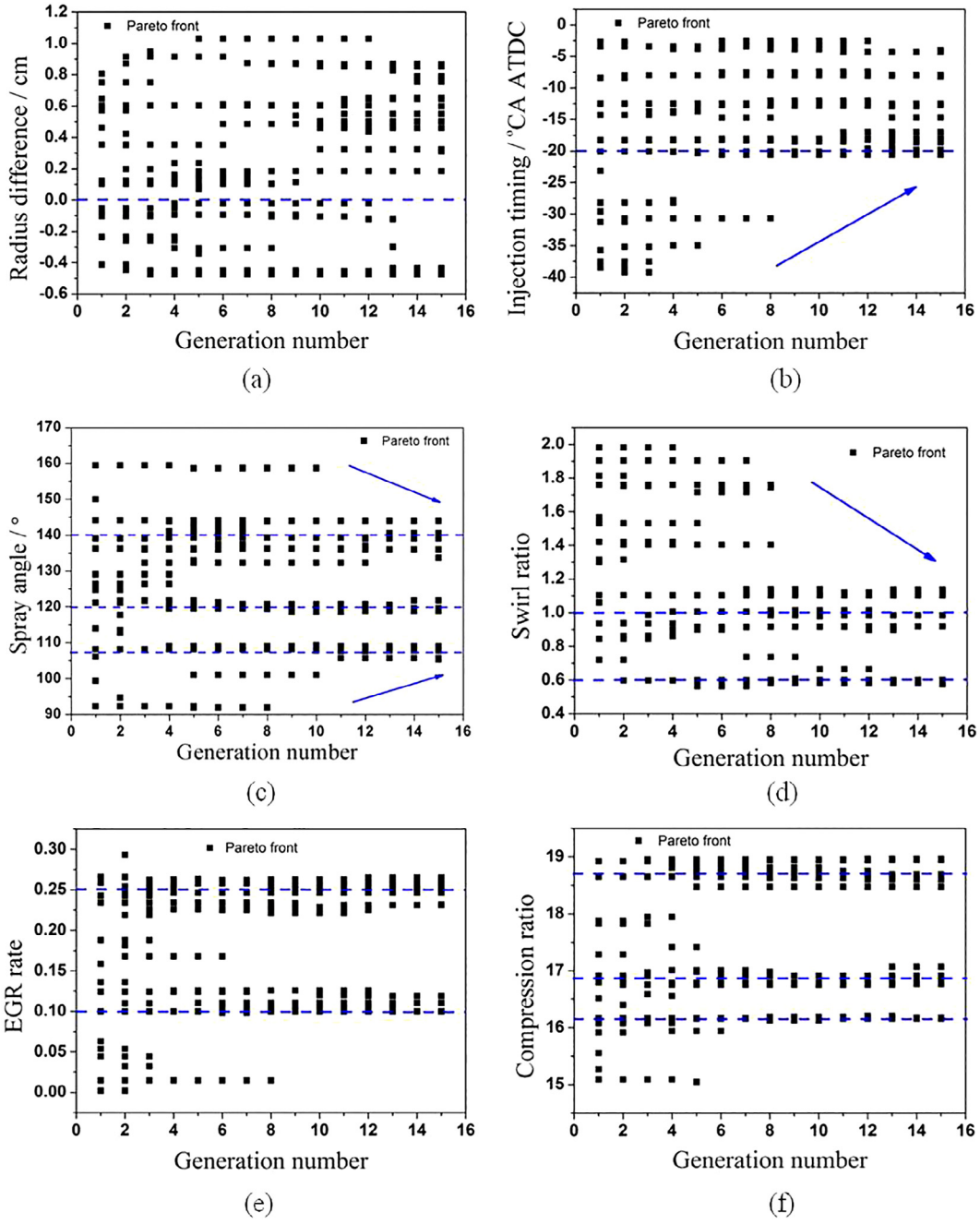

Fig. 12. Evolution of the optimized parameters on the Pareto front.

Table 6
Comparison of the parameters, emissions and ISFC.

Case NO.	TD mm	BD mm	IT °CA	SA °	CR	SR	EGR rate %	NO*x* g/kW·h	CH_4 g/kW·h	ISFC g/kW·h
1	4.66	4.48	−12.5	143.89	18.7	0.98	11	7.04	0.001	168.3
3	3.45	3.93	−7.9	108.93	16.9	0.60	25	1.66	9.52	205.6

NO*x* formation region follows the evolution of the high temperature region. In case 1, the NO*x* is almost produced in the entire combustion chamber as the compression ratio is high and the EGR rate is low. With the reduction of injection timing, compression ratio and increase of the EGR rate, the NO*x* is only produced at the bottom of the combustion chamber in case 3.

When the mixture temperature is over than 1700 K, the premixed CH_4 can be oxidized completely. At 20 °CA ATDC, almost all the CH_4 was consumed in case 1 as the high temperature region is distributed throughout the combustion chamber, whereas plenty of CH_4 is still exist in case 3. The CH_4 emission is mostly due to the retention of unburned fuel in the squish region and piston crevices in the cylinder. Where the flame quenching will occur in these regions as the higher surface-to-volume ratio increase the heat transfer and reduce the mixture

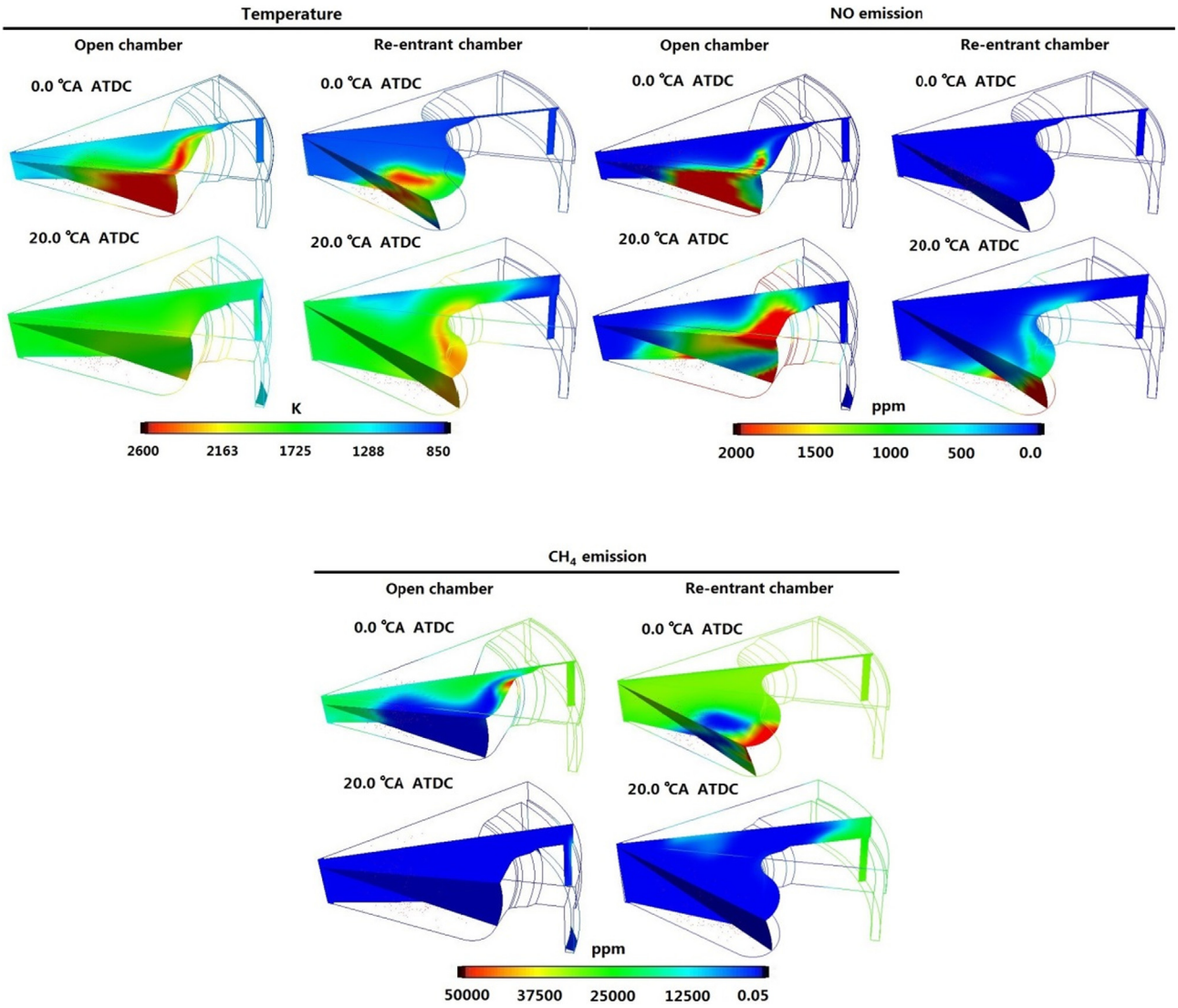

Fig. 13. Comparison of the temporal and spatial distribution of the temperature and pollutants.

temperature. The main method to achieve high thermal efficiency and low HC emission is to burn the fuel in the squish region completely. For the open chamber case (case 1), the throat radius is larger, which will promote the squish airflow into the combustion chamber and burned gas out of the combustion chamber into the squish. Therefore, the low temperature mixture in the squish region will blend with the higher temperature mixture in the combustion bowl region sufficiently and the mixture will burn completely [40,41].

5. Conclusion

The artificial intelligence method was combined with KIVA-3V code for the optimization of the performance and emissions characteristics of a dual fuel engine. The fuel injection parameters, operating parameters and combustion bowl profile are optimized simultaneously. The main conclusions are summarized as follows.

1. For Soot emission, almost all the solutions can meet the EURO VI emission limit. However, for NO*x* emission, only partial solutions can satisfy the EURO V emission limit.
2. More open combustion chambers are chosen than the re-entrant combustion chamber on the Pareto front. Excessive advancing fuel injection timing is not conducive to improving engine performance. The wide distribution of diesel fuel spray angle gradually concentrates to three locations, which are around 55°, 60° and 70°. The swirl ratio gradually degenerates to two points, which are around 0.6 and 1.0. The EGR rate is divided into two grades, which are around 0.1 and 0.25. Three compression ratios are favorable on the Pareto front, which are around 16.1, 16.8 and 18.7.
3. The minimum fuel consumption rate is observed at the center of the response surface for injection timing vs. EGR rate. The fuel consumption rate decreases with the increase of the injection angle, whereas it increases slightly with the increase of the swirl ratio.
4. With the advancing of the injection timing, the CH_4 emission decreases obviously. The CH_4 emission decreases slightly with small amount of EGR additions. However, CH_4 emission will increase when large amount of EGR was introduced. The CH_4 emissions are very high with very large or small swirl ratios. However, when the spray angle and the swirl ratio reach the maximum design value at the same time, CH_4 emission decreases obviously.
5. The retarded injection timing is the most influential parameter in achieving the reduced NO*x* emissions. The introduction of EGR rate has a moderate effect on the NO*x* emissions. Very high or low swirl ratio will both reduce the NO*x* emissions. NO*x* emissions increases very fast when the spray angle and the swirl ratio reach the maximum design value simultaneously.

6. The NO*x* emissions observed with the re-entrant combustion chamber is lower than that in the open combustion chamber cases, whereas the ISFC and CH_4 emissions are higher.

Declaration of Competing Interest

The authors declare that they have no known competing financial interests or personal relationships that could have appeared to influence the work reported in this paper.

Acknowledgement

This study is supported by the National Natural Science Foundation of China (NO. 51406007).

References

[1] Han S, Kim J, Bae C. Effect of air-fuel mixing quality on characteristics of conventionaland low temperature diesel combustion. Appl Energy 2014;119:454–66.
[2] Yang B, Wei X, Xi C, Liu Y, Zeng K, Lai MC. Experimental study of the effects of natural gas injection timing on the combustion performance and emissions of a turbocharged common rail dual-fuel engine. Energy Convers Manage 2014;87:297–304.
[3] Yang F, Yao C, Wang J, Ouyang M. Load expansion of a dieseline compression ignition engine with multi-mode combustion. Fuel 2016;171:5–17.
[4] Chen H, Xie B, Ma J, Chen Y. NO*x* emission of biodiesel compared to diesel: Higher or lower? Appl Therm Eng 2018;137:584–93.
[5] Chen H, Su X, He J, Xie B. Investigation on combustion and emission characteristics of a common rail diesel engine fueled with diesel/n-pentanol/methanol blends. Energy 2019;167(15):297–311.
[6] Poorghasemi K, Khoshbakhti Saray R, Ansari E, Irdmousa BK, Shahbakhti M, Naber JD. Effect of diesel injection strategies on natural gas/diesel RCCI combustion characteristics in a light duty diesel engine. Appl Energy 2017;199:430–46.
[7] Li Y, Li H, Guo H, Li Y, Yao M. A numerical investigation on methane combustion and emissions from a natural gas-diesel dual fuel engine using CFD model. Appl Energy 2017;205:153–62.
[8] Maciej M, Cemil B. Understanding the role of low reactivity fuel stratification in a dual fuel RCCI engine – a simulation study. Appl Energy 2017;191:689–708.
[9] Ma X, Zhang F, Xu H, Shuai S. Throttleless and EGR-controlled stoichiometric combustion in a diesel-gasoline dual-fuel compression ignition engine. Fuel 2014;115:765–77.
[10] Shu J, Fu J, Liu J, Ma Y, Wang S, Deng B, Zeng D. Effects of injector spray angle on combustion and emissions characteristics of a natural gas (NG)-diesel dual fuel engine based on CFD coupled with reduced chemical kinetic model. Appl Energy 2019:233–4. 182–195.
[11] Yousefi A, Guo H, Birouk M. Effect of swirl ratio on NG/diesel dual-fuel combustion at low to high engine load conditions. Appl Energy 2018;229:375–88.
[12] Yang B, Xi C, Wei X, Zeng K, Lai MC. Parametric investigation of natural gas port injection and diesel pilot injection on the combustion and emissions of a turbocharged common rail dual-fuel engine at low load. Appl Energy 2015;143:130–7.
[13] Shim E, Park H, Bae C. Intake air strategy for low HC and CO emissions in dual-fuel (CNG-diesel) premixed charge compression ignition engine. Appl Energy 2018;225:1068–77.
[14] Ryu K. Effects of pilot injection timing on the combustion and emissions characteristics in a diesel engine using biodiesel–CNG dual fuel. Appl Energy 2013;111:721–30.
[15] Liu J, Yang F, Wang H, Ouyang M, Hao S. Effects of pilot fuel quantity on the emissions characteristics of a CNG/diesel dual fuel engine with optimized pilot injection timing. Appl Energy 2013;110:201–6.
[16] Papagiannakis RG, Krishnan SR, Rakopoulos DC, Srinivasan KK, Rakopoulos CD. A combined experimental and theoretical study of diesel fuel injection timing and gaseous fuel/diesel mass ratio effects on the performance and emissions of natural gas-diesel HDDI engine operating at various loads. Fuel 2017;202:675–87.
[17] Yousefi A, Guo H, Birouk M. Effect of diesel injection timing on the combustion of natural gas/diesel dual-fuel engine at low-high load and low-high speed conditions. Fuel 2019;235:838–46.
[18] Yang B, Zeng K. Effects of natural gas injection timing and split pilot fuel injection strategy on the combustion performance and emissions in a dual-fuel engine fueled with diesel and natural gas. Energy Convers Manage 2018;168:162–9.
[19] Wang Z, Zhao Z, Wang D, Tan M, Han Y, Liu Z, et al. Impact of pilot diesel ignition mode on combustion and emissions characteristics of a diesel/natural gas dual fuel heavy-duty engine. Fuel 2016;167:248–56.
[20] Jung J, Song S, Hur KB. Numerical study on the effects of intake valve timing on performance of a natural gas-diesel dual-fuel engine and multi-objective Pareto optimization. Appl Therm Eng 2017;121:604–16.
[21] Gatts T, Liu S, Liew C, Ralston B, Bell C, Li H. An experimental investigation of incomplete combustion of gaseous fuels of a heavy-duty diesel engine supplemented with hydrogen and natural gas. Int J Hydrogen Energy 2012;37(9):7848–59.
[22] Lotfan S, Akbarpour Ghiasi R, Fallah M, Sadeghi MH. ANN-based modeling and reducing dual-fuel engine's challenging emissions by multi-objective evolutionary algorithm NSGA-II. Appl Energy 2016;175:91–9.
[23] Navid A, Khalilarya S, Taghavifar H. Comparing multi-objective non-evolutionary NLPQL and evolutionary genetic algorithm optimization of a DI diesel engine: DoE estimation and creating surrogate model. Energ Convers Manage 2016;126:385–99.
[24] Xu Z, Jia M, Li Y, Chang Y, Xu G, Xu L, et al. Computational optimization of fuel supply, syngas composition, and intake conditions for a syngas/diesel RCCI engine. Fuel 2018;234:120–34.
[25] Wang B, Li T, Ge L, Ogawa H. Optimization of combustion chamber geometry for natural gas engines with diesel micro-pilot-induced ignition. Energy Convers Manage 2016;122:552–63.
[26] Liu J, Wang J, Zhao H. Optimization of the injection parameters and combustion chamber geometries of a diesel/natural gas RCCI engine. Energy 2018;164:837–52.
[27] Deb M, Debbarma B, Majumder A, Banerjee R. Performance-emission optimization of a diesel-hydrogen dual fuel operation: A NSGA II coupled TOPSIS MADM approach. Energy 2016;117:281–90.
[28] Beale JC, Reitz RD. Modeling spray atomization with the kelvin helmholtz/rayleigh-taylor hybrid model. Atomization Sprays 1999;9:623–50.
[29] Munnannur A, Reitz RD. Comprehensive collision model for multidimensional engine spray computations. Atomization Sprays 2009;19:597–619.
[30] Mattarelli E, Rinaldini CA, Golovitchev VI. CFD-3D analysis of a light duty Dual Fuel (Diesel/Natural Gas) combustion engine. Energy Procedia 2014;45:929–37.
[31] Chen WM, Shuai SJ, Wang JX. A soot formation embedded reduced reaction mechanism for diesel surrogate fuel. Fuel 2009;88:1927–36.
[32] Yang J, Golovitchev VI, Redon P, López Sánchez JJ. Numerical Analysis of NOx Formation Trends in Biodiesel Combustion using Dynamic ϕ-T Parametric Maps. SAE 2011-01-1929.
[33] Lipatnikov AN, Chomiak J. Turbulent flame speed and thickness: phenomenology, evaluation, and application in multi-dimensional simulations. Prog. Energy Combust 2002;28:1–74.
[34] Liu J, Zhang X, Wang T, Zhang J, Wang H. Experimental and numerical study of the pollution formation in a diesel/CNG dual fuel engine. Fuel 2015;159:418–29.
[35] Deb K, Pratap A, Agarwal S, Meyarivan T. A fast and elitist multiobjective genetic algorithm: NSGA-II. IEEE Trans Evol Comput 2002;6(2):182–97.
[36] Deb K, Jain H. An evolutionary many-objective optimization algorithm using reference-point based non-dominated sorting approach, part i: solving problems with box constraints. IEEE Trans Evol Comput 2014;18(4):577–601.
[37] Hamosfakidis V, Reitz RD. Optimization of a hydrocarbon fuel ignition model for two single component surrogates of diesel fuel. Combust Flame 2003;132(3):433–50.
[38] Zhang J, Niu S, Zhang Y, Tang C, Jiang X, Hu E, et al. Experimental and modeling study of the auto-ignition of n-heptane/n-butanol mixtures. Combust Flame 2013;160(1):31–9.
[39] Jiang X, Zhang Y, Man X, Pan L, Huang Z. Shock tube measurements and kinetic study on ignition delay times of lean DME/n-butane blends at elevated pressures. Energ Fuel 2013;27(10):6238–46.
[40] Huang Z, Pan KY, Zhou LB, Jiang DM. Effects of top land widths and operating conditions on exhaust hydrocarbon emissions in a spark ignition engine. P I Mech Eng D-J Aut 1996;210(D3):243–7.
[41] Huang Z, Pang J, Pan K. Investigation on hydrocarbon emissions from crevice and oil layer during cold start and idling periods in SI engine. P I Mech Eng D-J Aut 1998;212(D5):501–5.